SUPPORTING INFORMATION

Advanced Use of High-Performance Liquid Chromatography for Synthesis of Controlled Metal Clusters

Yoshiki Niihori,[a] Miku Matsuzaki,[a] Chihiro Uchida,[a] and Yuichi Negishi*[,a,b]

[a]*Department of Applied Chemistry, Faculty of Science, Tokyo University of Science, 1-3 Kagurazaka, Shinjuku-ku, Tokyo 162-8601, Japan*
[b]*Photocatalysis International Research Center, Tokyo University of Science, 2641 Yamazaki, Noda, Chiba 278-8510, Japan*

I. Synthesis

Chemicals

All chemicals were purchased commercially and used as received without further purification. Hydrogen tetrachloroaurate tetrahydrate ($HAuCl_4 \cdot 4H_2O$) was obtained from Tanaka Kikinzoku. Palladium sodium chloride trihydrate ($PdCl_2 \cdot 2NaCl \cdot 3H_2O$), tetraoctylammonium bromide ($(C_8H_{17})_4NBr$), sodium tetrahydroborate ($NaBH_4$), octanethiol ($C_8H_{17}SH$), decanethiol ($C_{10}H_{21}SH$), dodecanethiol ($C_{12}H_{25}SH$), methanol, acetone, toluene, dichloromethane, acetonitrile, and tetrahydrofuran (THF) were obtained from Wako Pure Chemical Industries Ltd. Butanethiol (C_4H_9SH), hexanethiol ($C_6H_{13}SH$), and phenylethanethiol (PhC_2H_4SH) were purchased from Tokyo Kasei. 4-*tert*-Butylphenylmethanethiol (^{t}BuPhCH$_2$SH, Chart S1) and tetradecanethiol ($C_{14}H_{29}SH$) were purchased from Aldrich. 4-Bromophenylmethanethiol (BrPhCH$_2$SH, Chart S1) was purchased from Fluorochem. The matrix, *trans*-2-[3-(4-*tert*-butylphenyl)-2-methyl-2-propenylidene]malononitrile (DCTB), was purchased from Santa Cruz Biotechnology. Didodecyl diselenide ($(C_{12}H_{25}Se)_2$) was synthesized in our laboratory using literature methods.[1,2] Deionized water with a resistivity greater than 18.2 MΩ cm was used.

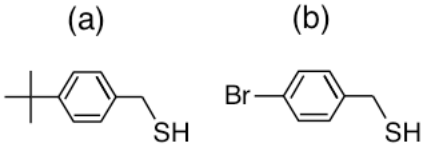

Chart S1. Molecular structures of (a) 4-*tert*-butylphenylmethanethiol (^{t}BuPhCH$_2$SH) and (b) 4-bromophenylmethanethiol (BrPhCH$_2$SH).

II. Characterization

High-performance liquid chromatography (HPLC) experiments using reverse-phase column

HPLC experiments were conducted using a Shimadzu instrument consisting of a DGU-20A3R on-line degasser, LC-20AD pump, CTO-20AC column oven, and SPD-M20A photodiode array (PDA) detector (Chart S2). In all the experiments, a stainless-steel column (250 mm × 4.6 mm i.d.) packed with 5 μm C18-bonded silica with pores of size 175 Å (Hypersil C18, Thermo Scientific) was used as the reverse-phase column because this column separates the clusters better than other reverse-phase columns, a stainless steel column (250 mm × 4.6 mm i.d.) packed with 5 μm C8-bonded silica with pores of size 130 Å (Hypersil C8, Thermo Scientific), and a stainless-steel column (150 mm × 4.6 mm i.d.) packed with 5 μm phenyl-bonded silica of pore size 130 Å (Hypersil Phenyl, Thermo Scientific; Figure S17 and Table S1). The column temperature was fixed at 25 °C to maintain reproducibility (Figure S18 and Table S2). Before sample injection, aging (stabilization) of the column and detector was performed for a sufficient time. The absorbance chromatogram was monitored, using the PDA, at 380 nm. Each sample was first diluted in THF (0.1 mg/5 μL) and then suspended in solution by adding methanol (15 μL). Then the sample suspension (20 μL) was injected into the instrument with a methanol mobile phase at a flow rate of 1 mL/min. After sample

injection, the amount of THF in the mobile phase was continuously increased, using a gradient program that increased the [THF]/[methanol] ratio of the mobile phase from 0% to 100%, with a replacement time of 40 min (Chart 2). Several other combinations of mobile-phase solvents were also tested. However, better separation was not achieved for the other combinations listed in Tables S3 and S4 using the gradient program in Chart 2 (Figures S19 and S20). After analysis, the chromatogram was corrected by subtracting the background measured without a sample.

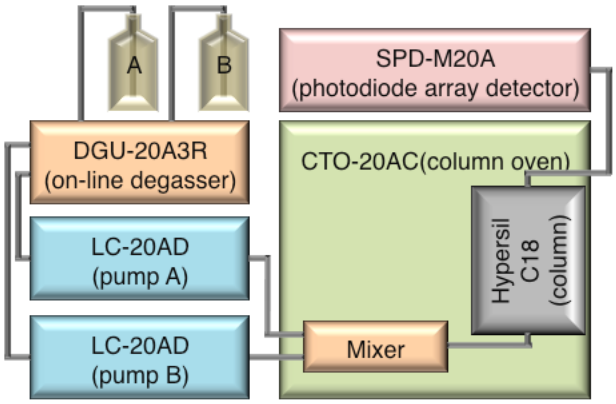

Chart S2. HPLC system used in this work.

Matrix-assisted laser desorption–ionization (MALDI) mass spectrometry

MALDI mass spectra were acquired with a time-of-flight mass spectrometer (JEOL Ltd., JMS-S3000) using an Nd:YAG laser (wavelength: 349 nm) and DCTB as the MALDI matrix. The cluster-to-matrix ratio was set at 1:1000. The laser fluence was reduced to the lowest value that enabled ions to be detected. All the spectra were obtained in negative-ion mode.

Analysis of separation resolution

The separation resolution (R_s) was calculated using the following equation:[3]

$$R_s = 2\frac{t_B - t_A}{W_B + W_A} \quad (1)$$

In this equation, t_A and t_B are the retention times of peaks A and peak B, respectively (Chart S3), and W_A and W_B are the full widths of peaks A and B, respectively (Chart S3). In the calculation, the objective peak and the next intense peak were used for estimating R_s of each peak.

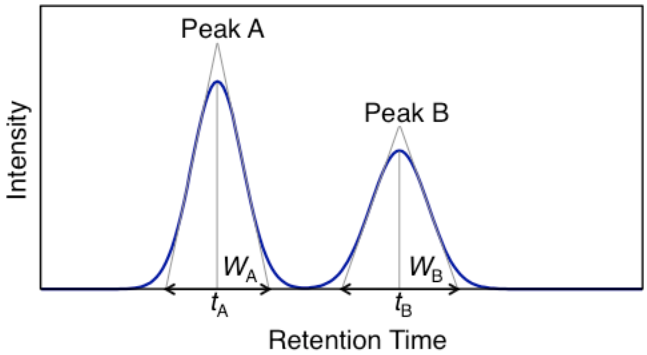

Chart S3. Parameters used for calculation of resolution, R_s.

III. Results

Table S1. Column Dependence of Resolution (R_s)

Column[a]	x[b]	t_R (min)[c]	R_s[d]
Hypersil C18	0	31.7	1.59
	1	31.4	1.59
	2	31.0	1.54
	3	30.7	1.41
	4	30.3	1.31
	5	29.8	
Hypersil C8	0	29.2	1.26
	1	28.9	1.29
	2	28.6	1.37
	3	28.2	1.35
	4	27.9	1.39
	5	27.5	

[a]The column temperature was fixed at 25 °C. Methanol and THF were used as the adsorption and elution solvents (Chart 1), respectively. [b]The peak number of peaks observed in the chromatograms of $Au_{24}Pd(SC_{12}H_{25})_{18-x}(SCH_2Ph^tBu)_x$ (Figure S17). The peak x represents the peak from $Au_{24}Pd(SC_{12}H_{25})_{18-x}(SCH_2Ph^tBu)_x$. [c]The retention time of each peak. [d]The resolution was calculated using eq. (1). A higher value indicates better resolution.

Table S2. Temperature Dependence of Resolution (R_s)

Temperature[a]	x[b]	t_R (min)[c]	R_s[d]
0 °C	0	34.7	1.36
	1	34.4	1.34
	2	34.0	1.31
	3	33.6	1.22
	4	33.2	1.11
	5	32.8	
25 °C	0	31.7	1.59
	1	31.4	1.59
	2	31.0	1.54
	3	30.7	1.41
	4	30.3	1.31
	5	29.8	
50 °C	0	29.0	1.66
	1	28.7	1.65
	2	28.3	1.60
	3	28.0	1.59
	4	27.6	1.43
	5	27.2	

[a]Hypersil C18 column was used as the reverse-phase column. Methanol and THF were used as the adsorption and elution solvents, respectively. [b]The peak number of the peaks observed in the chromatograms of $Au_{24}Pd(SC_{12}H_{25})_{18-x}(SCH_2Ph^tBu)_x$ (Figure S18). The peak x represents the peak from $Au_{24}Pd(SC_{12}H_{25})_{18-x}(SCH_2Ph^tBu)_x$. [c]The retention times of each peak. [d]The resolution was calculated using eq. (1). A higher value indicates better resolution.

Table S3. Adsorption Solvent Dependence of Resolution (R_s).

Solvent[a]	x[b]	t_R (min)[c]	R_s[d]
acetonitrile	0	35.6	1.71
	1	35.3	1.55
	2	35.0	1.43
	3	34.6	1.29
	4	34.3	1.14
	5	33.9	
methanol	0	31.7	1.59
	1	31.4	1.59
	2	31.0	1.54
	3	30.7	1.41
	4	30.3	1.31
	5	29.8	
ethanol	0	29.3	1.55
	1	29.0	1.38
	2	28.6	1.32
	3	28.2	1.22
	4	27.7	1.13
	5	27.3	

[a]Hypersil C18 column was used as the reverse-phase column. The column temperature was fixed at 25 °C. THF was used as the elution solvent. [b]The peak number of the peaks observed in the chromatograms of $Au_{24}Pd(SC_{12}H_{25})_{18-x}(SCH_2Ph^tBu)_x$ (Figure S19). The peak x represents the peak from $Au_{24}Pd(SC_{12}H_{25})_{18-x}(SCH_2Ph^tBu)_x$. [c]The retention times of each peak. [d]The resolution was calculated using eq. (1). A higher value indicates better resolution.

Table S4. Elution Solvent Dependence of Resolution (R_s)

Solvent[a]	x[b]	t_R (min)[c]	R_s[d]
dichloromethane	0	34.7	1.16
	1	34.4	1.08
	2	34.1	0.954
	3	33.8	0.827
	4	33.5	0.720
	5	33.2	
benzene	0	33.5	1.04
	1	33.2	0.983
	2	33.0	0.896
	3	32.8	0.807
	4	32.5	0.715
	5	32.3	
toluene	0	32.8	0.849
	1	32.6	0.722
	2	32.4	0.592
	3	32.2	0.536
	4	31.9	0.514
	5	31.7	
tetrahydrofuran (THF)	0	31.7	1.59
	1	31.4	1.59
	2	31.0	1.54
	3	30.7	1.41
	4	30.3	1.31
	5	29.8	

[a]Hypersil C18 column was used as the reverse-phase column. The column temperature was fixed at 25 °C. Methanol was used as the adsorption solvent. [b]The peak number of the peaks observed in the chromatograms of $Au_{24}Pd(SC_{12}H_{25})_{18-x}(SCH_2Ph^tBu)_x$ (Figure S20). The peak x represents the peak from $Au_{24}Pd(SC_{12}H_{25})_{18-x}(SCH_2Ph^tBu)_x$. [c]The retention time of each peak. [d]The resolution was calculated using eq. (1). A higher value indicates better resolution.

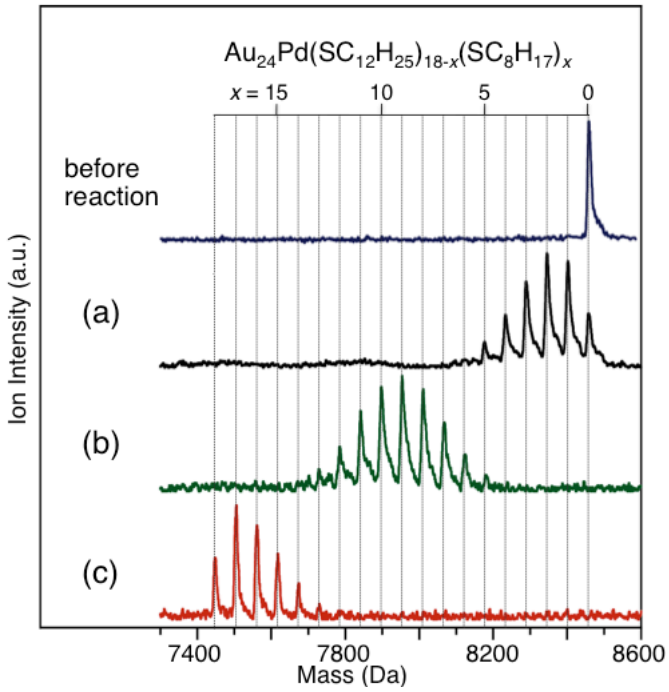

Figure S1. Negative-ion MALDI mass spectra of product formed by reaction between $Au_{24}Pd(SC_{12}H_{25})_{18}$ and $C_8H_{17}SH$ (entry 1 in Table 1) with reaction conditions ($[C_8H_{17}SH]/[Au_{24}Pd(SC_{12}H_{25})_{18}]$ ratio, reaction time) = (a) 100, 5 s, (b) 200, 5 min, and (c) 1000, 20 min. In the MALDI mass spectra and chromatograms (Figure 1), the same color indicates the same sample.

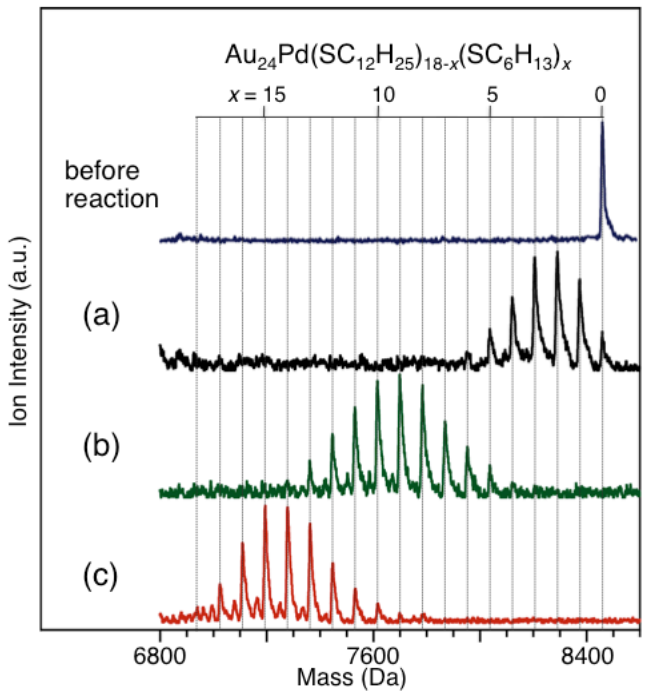

Figure S2. Negative-ion MALDI mass spectra of product formed by reaction between $Au_{24}Pd(SC_{12}H_{25})_{18}$ and $C_6H_{13}SH$ (entry 2 in Table 1) with reaction conditions ($[C_6H_{13}SH]/[Au_{24}Pd(SC_{12}H_{25})_{18}]$ ratio, reaction time) = (a) 100, 5 s, (b) 200, 5 min, and (c) 1000, 20 min. In the MALDI mass spectra and chromatograms (Figure 1), the same color indicates the same sample.

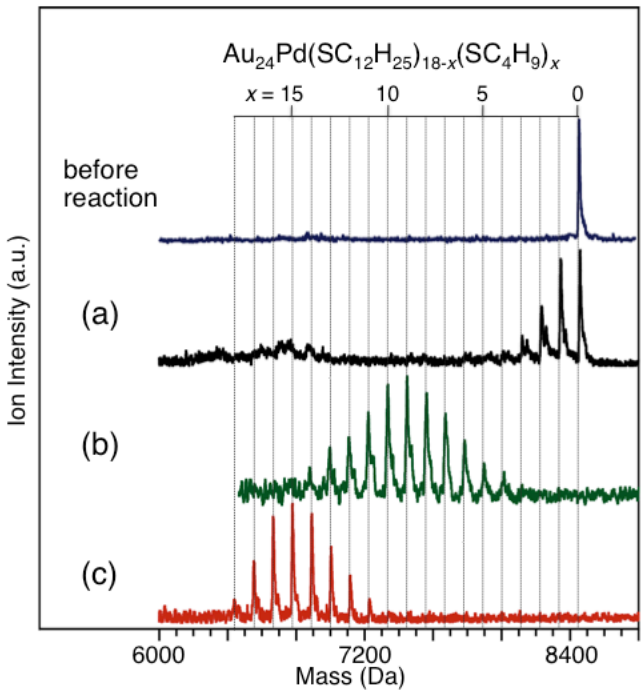

Figure S3. Negative-ion MALDI mass spectra of product formed by reaction between $Au_{24}Pd(SC_{12}H_{25})_{18}$ and C_4H_9SH (entry 3 in Table 1) with reaction conditions ($[C_4H_9SH]/[Au_{24}Pd(SC_{12}H_{25})_{18}]$ ratio, reaction time) = (a) 100, 5 s, (b) 200, 5 min, and (c) 1000, 20 min. In the MALDI mass spectra and chromatograms (Figure 1), the same color indicates the same sample.

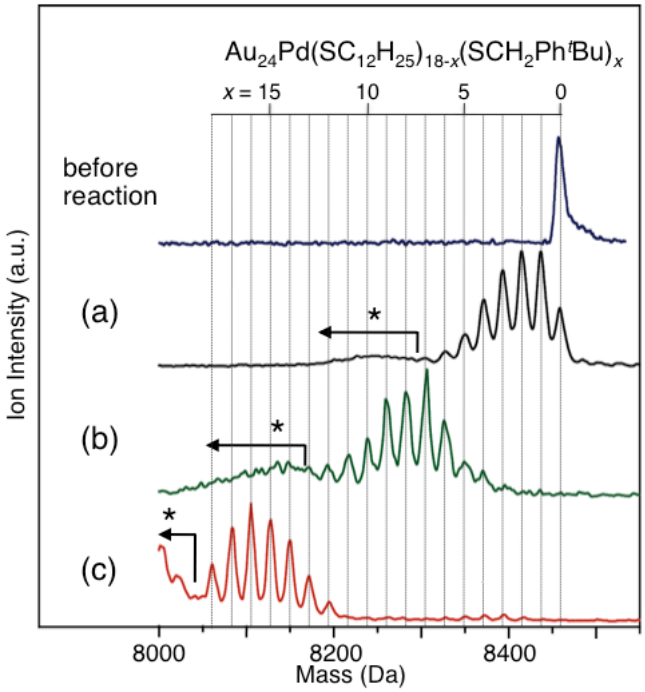

Figure S4. Negative-ion MALDI mass spectra of product formed by reaction between $Au_{24}Pd(SC_{12}H_{25})_{18}$ and $^tBuPhCH_2SH$ (entry 4 in Table 1) with reaction conditions ($[^tBuPhCH_2SH]/[Au_{24}Pd(SC_{12}H_{25})_{18}]$ ratio, reaction time) = (a) 100, 5 s, (b) 200, 5 min, and (c) 1000, 20 min. In the MALDI mass spectra and chromatograms (Figure 1), the same color indicates the same sample. Asterisks indicate the laser-induced fragments $[Au_{24}Pd(SC_{12}H_{25})_{18-x}(SCH_2Ph^tBu)_{x-1}S]$. These fragments were observed even with low laser fluence for $Au_{24}Pd(SC_{12}H_{25})_{18-x}(SCH_2Ph^tBu)_x$ and $Au_{24}Pd(SC_{12}H_{25})_{18-x}(SCH_2PhBr)_x$ (Figure S5).

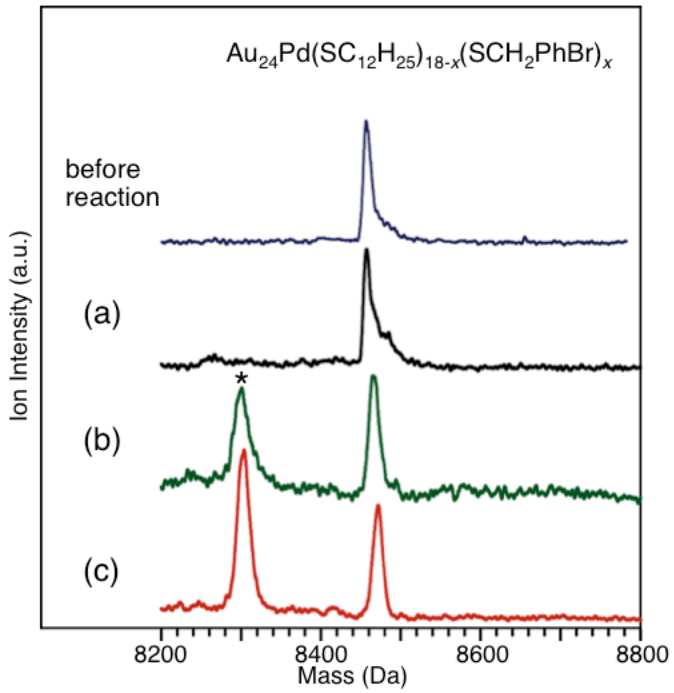

Figure S5. Negative-ion MALDI mass spectra of product formed by reaction between $Au_{24}Pd(SC_{12}H_{25})_{18}$ and $BrPhCH_2SH$ (entry 5 in Table 1) with reaction conditions ($[BrPhCH_2SH]/[Au_{24}Pd(SC_{12}H_{25})_{18}]$ ratio, reaction time) = (a) 100, 5 s, (b) 200, 5 min, and (c) 1000, 20 min. In the MALDI mass spectra and chromatograms (Figure 1), the same color indicates the same sample. Asterisks indicate laser-induced fragments $[Au_{24}Pd(SC_{12}H_{25})_{18-x}(SCH_2PhBr)_{x-1}S]$.

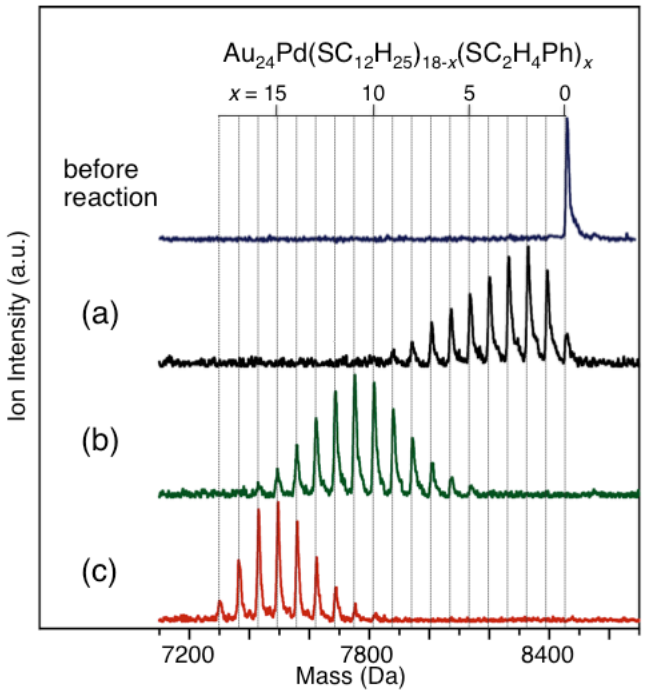

Figure S6. Negative-ion MALDI mass spectra of product formed by reaction between $Au_{24}Pd(SC_{12}H_{25})_{18}$ and PhC_2H_4SH (entry 6 in Table 1) with reaction conditions ($[PhC_2H_4SH]/[Au_{24}Pd(SC_{12}H_{25})_{18}]$ ratio, reaction time) = (a) 100, 5 s, (b) 200, 5 min, and (c) 1000, 20 min. In the MALDI mass spectra and chromatograms (Figure 1), the same color indicates the same sample.

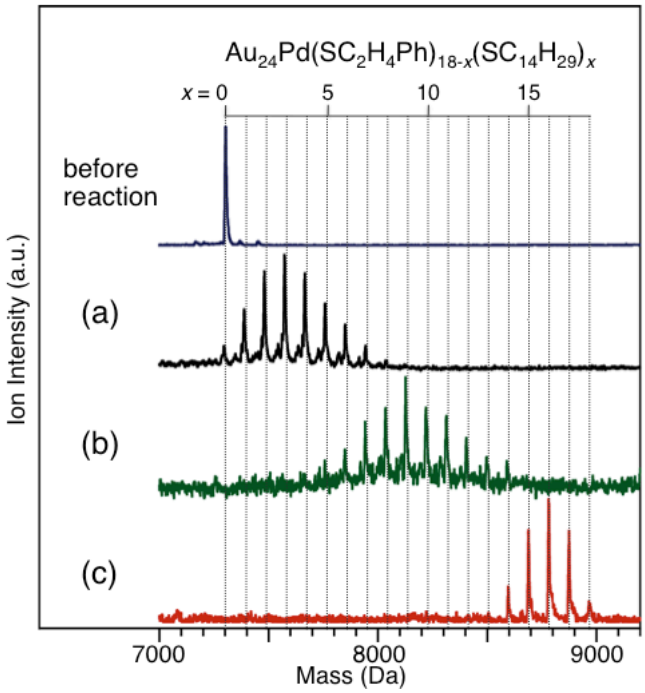

Figure S7. Negative-ion MALDI mass spectra of product formed by reaction between $Au_{24}Pd(SC_2H_4Ph)_{18}$ and $C_{14}H_{29}SH$ (entry 7 in Table 1) with reaction conditions ($[C_{14}H_{29}SH]/[Au_{24}Pd(SC_2H_4Ph)_{18}]$ ratio, reaction time) = (a) 100, 5 s, (b) 200, 5 min, and (c) 1000, 20 min. In the MALDI mass spectra and chromatograms (Figure 1), the same color indicates the same sample.

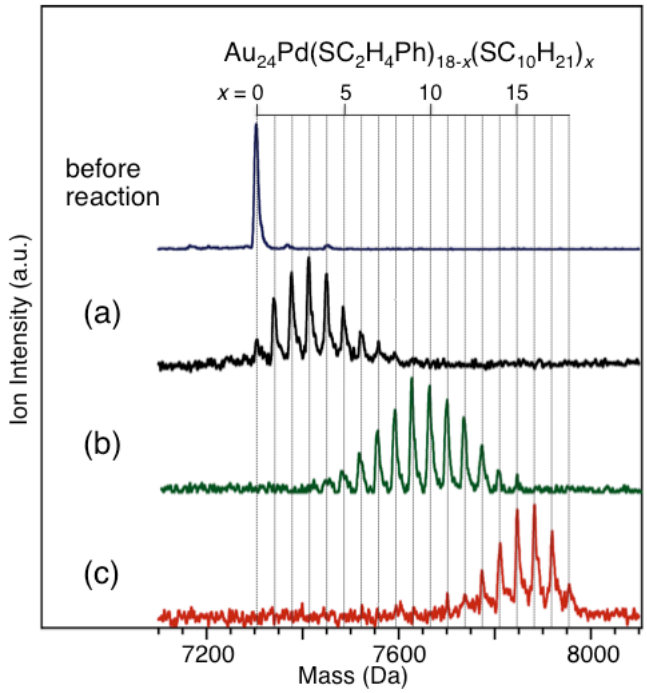

Figure S8. Negative-ion MALDI mass spectra of product formed by reaction between $Au_{24}Pd(SC_2H_4Ph)_{18}$ and $C_{10}H_{21}SH$ (entry 8 in Table 1) with reaction conditions ($[C_{10}H_{21}SH]/[Au_{24}Pd(SC_2H_4Ph)_{18}]$ ratio, reaction time) = (a) 100, 5 s, (b) 200, 5 min, and (c) 1000, 20 min. In the MALDI mass spectra and chromatograms (Figure 1), the same color indicates the same sample.

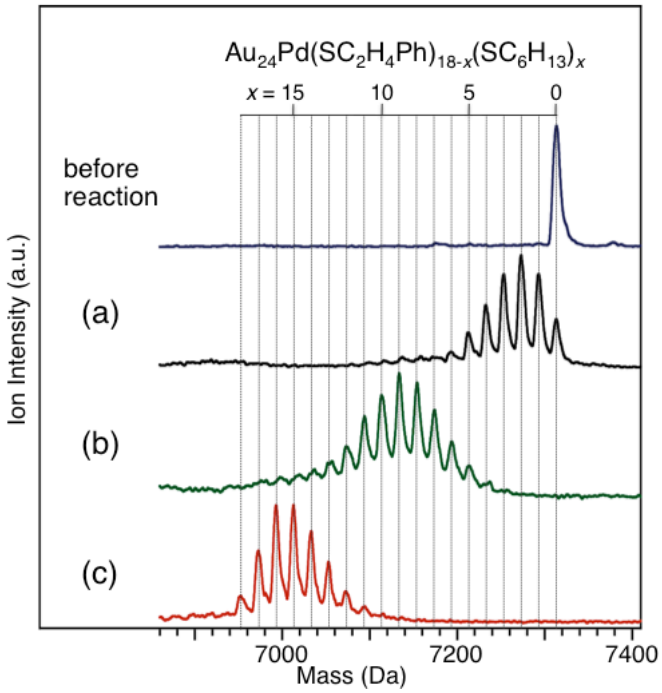

Figure S9. Negative-ion MALDI mass spectra of product formed by reaction between $Au_{24}Pd(SC_2H_4Ph)_{18}$ and $C_6H_{13}SH$ (entry 9 in Table 1) with reaction conditions ($[C_6H_{13}SH]/[Au_{24}Pd(SC_2H_4Ph)_{18}]$ ratio, reaction time) = (a) 100, 5 s, (b) 200, 5 min, and (c) 1000, 20 min. In the MALDI mass spectra and chromatograms (Figure 1), the same color indicates the same sample.

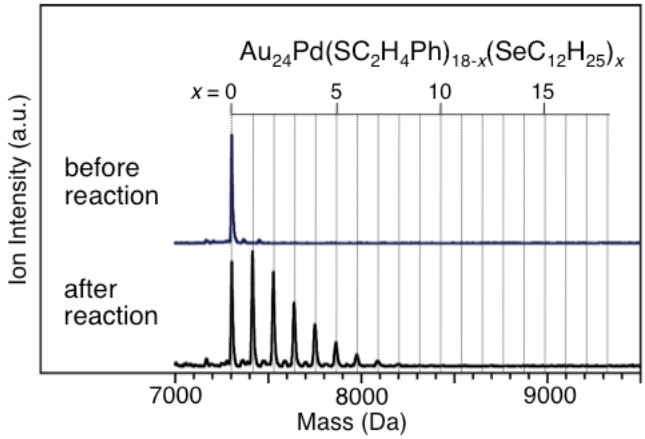

Figure S10. Negative-ion MALDI mass spectra of product formed by reaction between $Au_{24}Pd(SC_2H_4Ph)_{18}$ and $(C_{12}H_{25}Se)_2$ (entry 10 in Table 1) with reaction conditions ($[(C_{12}H_{25}Se)_2]/[Au_{24}Pd(SC_2H_4Ph)_{18}]$ ratio, reaction time) = 100, 5 s. $Au_{24}Pd(SC_2H_4Ph)_{18-x}(SeC_{12}H_{25})_x$ clusters were also synthesized using experimental conditions suitable for $Au_{24}Pd(SC_2H_4Ph)_{18-x}(SeC_{12}H_{25})_x$ with larger x values. However, the ion intensities of these clusters were very weak, and therefore reliable mass spectra were not observed.

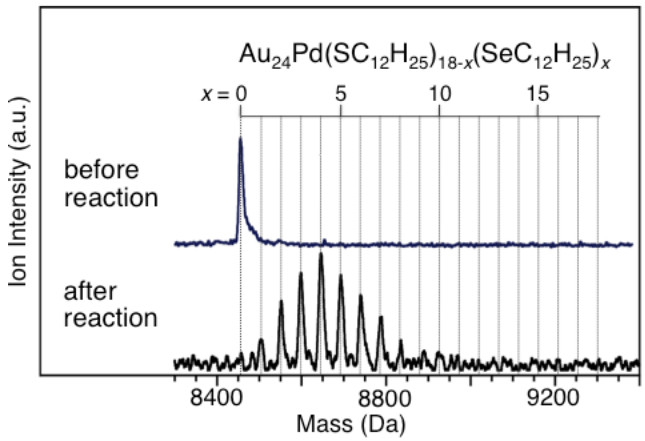

Figure S11. Negative-ion MALDI mass spectra of product formed by reaction between $Au_{24}Pd(SC_{12}H_{25})_{18}$ and $(C_{12}H_{25}Se)_2$ (entry 11 in Table 1) with reaction conditions ($[(C_{12}H_{25}Se)_2]/[Au_{24}Pd(SC_{12}H_{25})_{18}]$ ratio, reaction time) = 100, 5 s. $Au_{24}Pd(SC_{12}H_{25})_{18-x}(SeC_{12}H_{25})_x$ clusters were also synthesized using experimental conditions suitable for $Au_{24}Pd(SC_{12}H_{25})_{18-x}(SeC_{12}H_{25})_x$ with larger x values. However, the ion intensities of these clusters were very weak, and therefore reliable mass spectra were not observed.

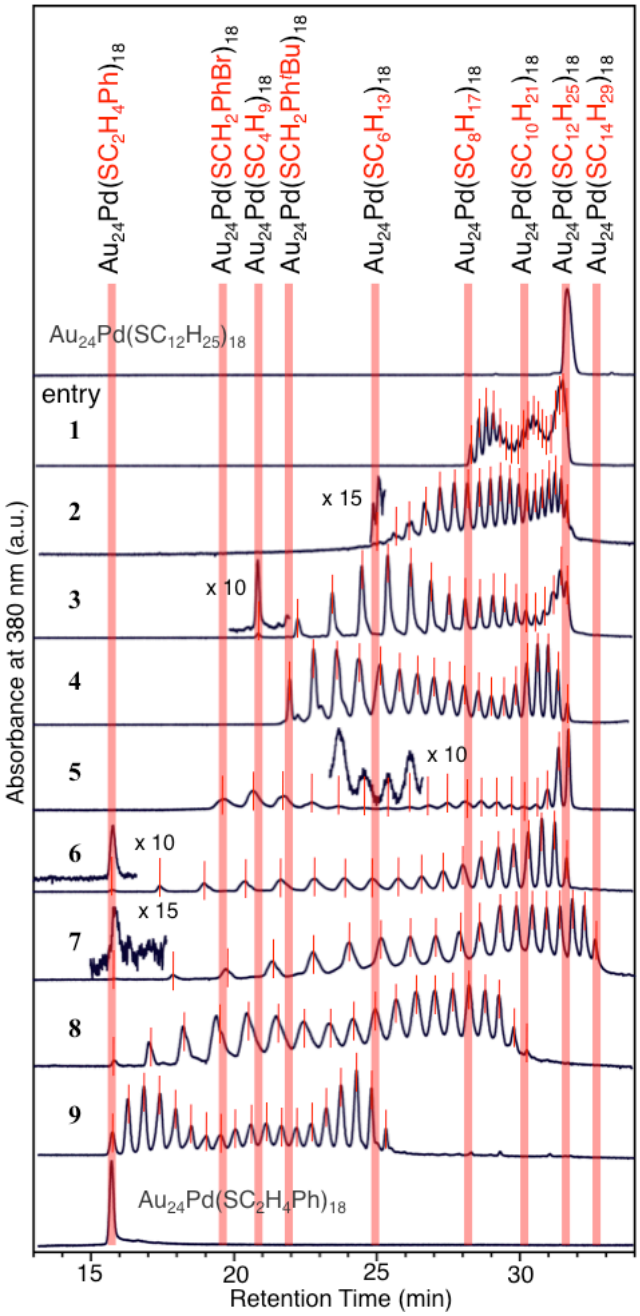

Figure S12. Summary of chromatograms of $Au_{24}Pd(SR_1)_{18-x}(SR_2)_x$ (x = 0–18) with ligand combinations of Table 1, entries 1–9 together with those of $Au_{24}Pd(SC_{12}H_{25})_{18}$ and $Au_{24}Pd(SC_2H_4Ph)_{18}$ for comparison. In these experiments, mixtures of three samples of $Au_{24}Pd(SR_1)_{18-x}(SR_2)_x$, shown in Figures S1–S9, were used for the separation. The broad red vertical lines indicate the retention times estimated for $Au_{24}Pd$ clusters protected with one type of ligand, $Au_{24}Pd(SR_1)_{18}$ and $Au_{24}Pd(SR_2)_{18}$. The narrow red vertical lines indicate the retention times of each peak. The number of peaks observed in each chromatogram is 19 in all cases, indicating that all ligand combinations of $Au_{24}Pd(SR_1)_{18-x}(SR_2)_x$ were separated for $Au_{24}Pd(SR_1)_{18-x}(SR_2)_x$ of entries 1–9.

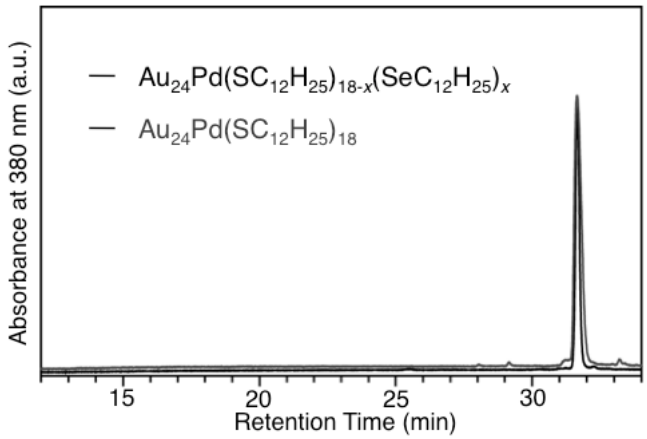

Figure S13. Chromatogram of $Au_{24}Pd(SC_{12}H_{25})_{18-x}(SeC_{12}H_{25})_x$ (x = 0–8) and that of $Au_{24}Pd(SC_{12}H_{25})_{18}$ for comparison. The chromatogram of $Au_{24}Pd(SC_{12}H_{25})_{18-x}(SeC_{12}H_{25})_x$ (x = 0–8) exhibits only one peak, and the retention time of this peak is consistent with that of $Au_{24}Pd(SC_{12}H_{25})_{18}$, indicating that the difference between the Au–ligand charge transfer little affects the polarity of the cluster surface.

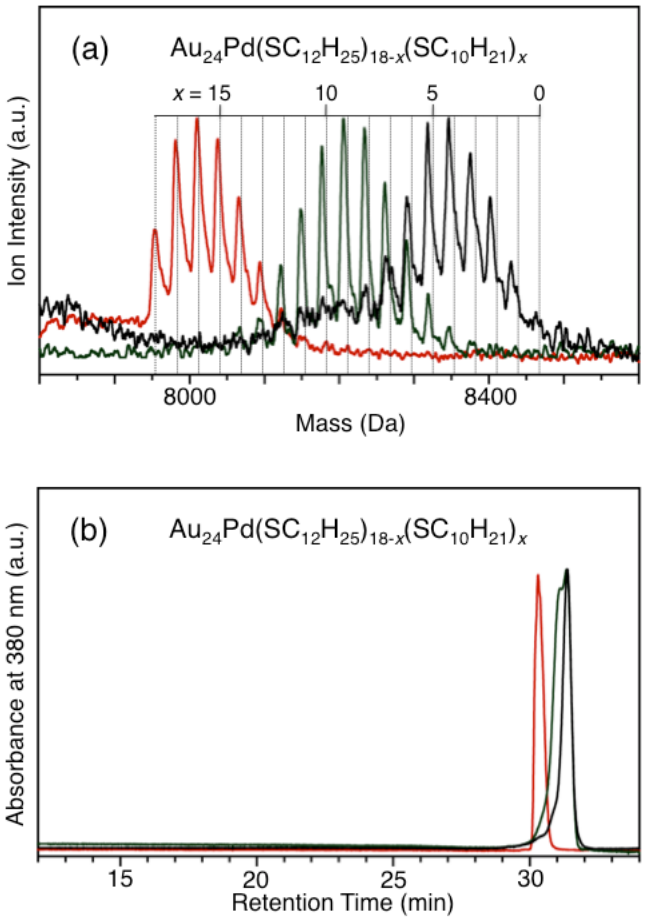

Figure S14. (a) Negative-ion MALDI mass spectra and (b) chromatograms of $Au_{24}Pd(SC_{12}H_{25})_{18-x}(SC_{10}H_{21})_x$ (x = 0–18). These results indicate that $Au_{24}Pd(SC_{12}H_{25})_{18-x}(SC_{10}H_{21})_x$ (x = 0–18) clusters are not separated using the linear-gradient program for solvent substitution.

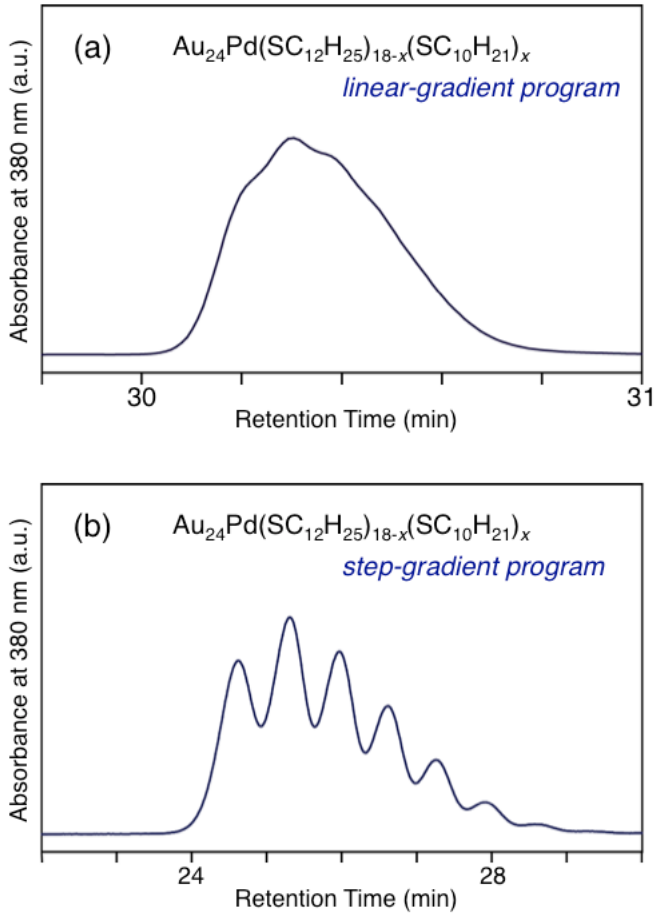

Figure S15. Comparison between (a) chromatogram obtained with linear-gradient program and (b) chromatogram obtained with step-gradient program for $Au_{24}Pd(SC_{12}H_{25})_{18-x}(SC_{10}H_{21})_x$ (x = 12–18; Figure 3a). In the experiment in (b), the step height was set at [50]. Accordingly, the retention times of each peak are shorter than those observed in the chromatogram in Figure 3(c), but each peak of $Au_{24}Pd(SC_{12}H_{25})_{18-x}(SC_{10}H_{21})_x$ is still separated under these conditions. These results imply that the peak separation observed in the chromatogram in Figure 3(c) is not caused simply by lengthening of the retention time.

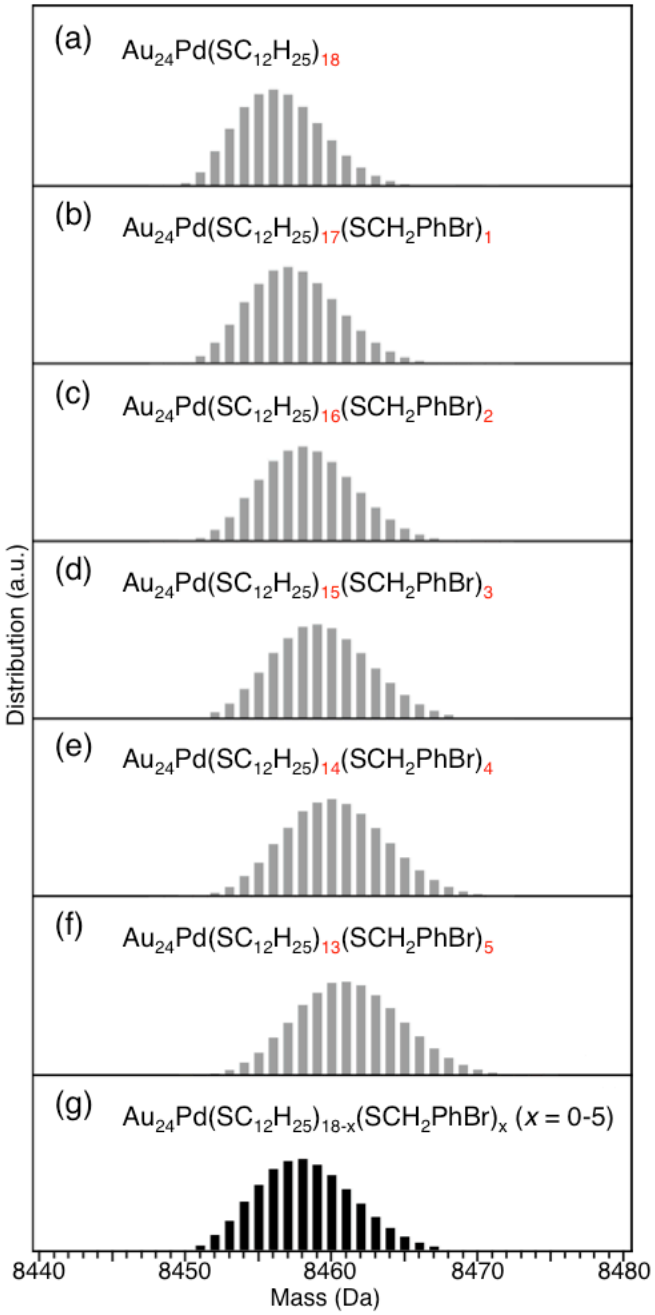

Figure S16. Isotope patterns of (a) $Au_{24}Pd(SC_{12}H_{25})_{18}$, (b) $Au_{24}Pd(SC_{12}H_{25})_{17}(SCH_2PhBr)_1$, (c) $Au_{24}Pd(SC_{12}H_{25})_{16}(SCH_2PhBr)_2$, (d) $Au_{24}Pd(SC_{12}H_{25})_{15}(SCH_2PhBr)_3$, (e) $Au_{24}Pd(SC_{12}H_{25})_{14}(SCH_2PhBr)_4$, and (f) $Au_{24}Pd(SC_{12}H_{25})_{13}(SCH_2PhBr)_5$, calculated using "Bunshiro" software The mass distributions of (a)–(f) are similar to each other. (g) Isotope patterns of $Au_{24}Pd(SC_{12}H_{25})_{18-x}(SCH_2PhBr)_x$ with distribution of (a):(b):(c):(d):(e):(f): = 0.125:0.290:0.310:0.190:0.072:0.013, which is the intensity ratio of $Au_{24}Pd(SC_{12}H_{25})_{18-x}(SCH_2PhBr)_x$ in the chromatogram (black line in Figure 6b). It is difficult to estimate the quantity of each constituent, (a)–(f), from (g).

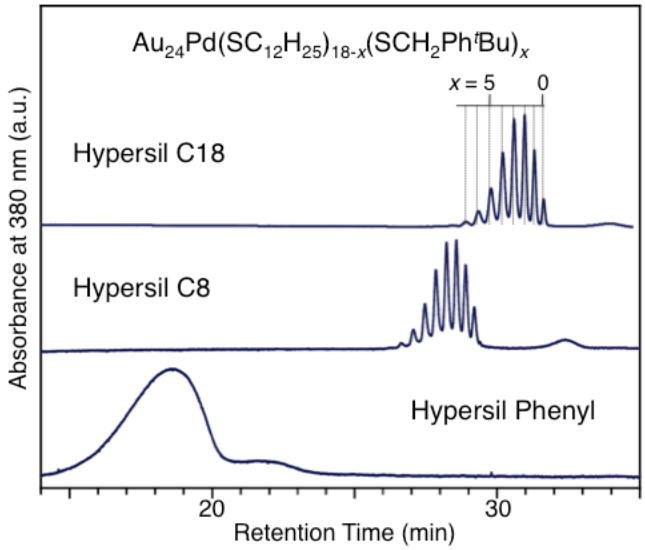

Figure S17. Column dependence of chromatograms. In these experiments, $Au_{24}Pd(SC_{12}H_{25})_{18-x}(SCH_2Ph^tBu)_x$ (x = 0–7) clusters with the distribution shown by the black line in Figure S4 were used. The column temperature was fixed at 25 °C. Methanol and THF were used as the adsorption and elution solvents, respectively (Chart 1). Each peak of the chromatogram obtained with the C18 column was assigned as indicated in the figure based on the MALDI mass spectrum of each fraction in a previous study; note that SCH_2Ph^tBu was abbreviated as SBB in the previous paper.[4] The resolutions of each chromatogram, calculated using eq. (1), are summarized in Table S1. The C18 column and C8 column separated the clusters with high resolution. Close inspection revealed that the former separates the clusters better than the latter (Table S1). The C18 column interacts with hydrophobic materials more strongly than the C8 column does, which leads to longer retention times and better separation of $Au_{24}Pd(SC_{12}H_{25})_{18-x}(SCH_2Ph^tBu)_x$. The clusters were not separated with high resolution by the phenyl column. Based on these results, we conducted all the other studies using the C18 column as the reverse-phase column.

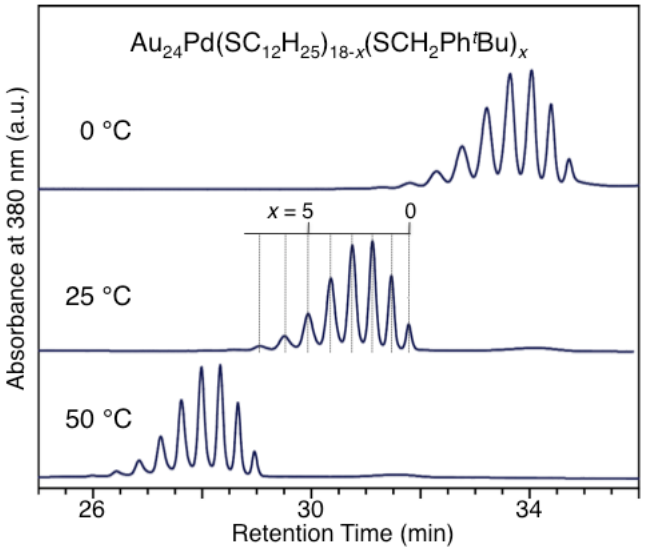

Figure S18. Temperature dependence of chromatograms. In these experiments, $Au_{24}Pd(SC_{12}H_{25})_{18-x}(SCH_2Ph^tBu)_x$ (x = 0–7) clusters with the distribution shown by the black line in Figure S4 were used. Methanol and THF were used as adsorption and elution solvents, respectively (Chart 1). The resolutions of each chromatogram are summarized in Table S2. An increase in the temperature decreased the retention time and increased the resolution (Table S2); these are general phenomena for HPLC.[5] However, the increase in resolution with increasing temperature was very slight. Furthermore, the clusters become unstable at high temperature.[6] We therefore conducted all other studies at a fixed temperature of 25 °C, which is the normal experimental condition.

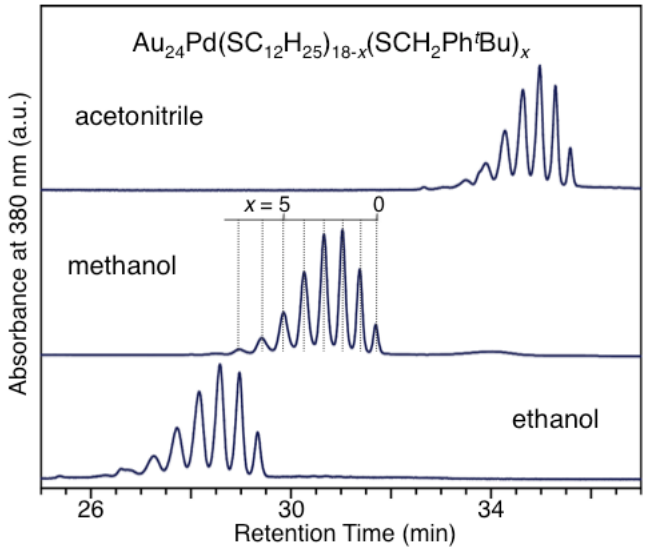

Figure S19. Adsorption solvent dependence of chromatograms. In these experiments, $Au_{24}Pd(SC_{12}H_{25})_{18-x}(SCH_2Ph^tBu)_x$ (x = 0–7) clusters with a distribution similar to that shown by the black line in Figure S4 were used. THF was used as the elution solvent (Chart 1). The resolutions are summarized in Table S3. The use of acetonitrile instead of methanol increased the retention time. However, the resolution decreased slightly (Table S3). The use of ethanol decreased the retention time and accordingly decreased the resolution (Table S3). Thus, with the gradient program in Chart 2 and THF as the elution solvent, the best resolution was obtained when methanol was used as the adsorption solvent.

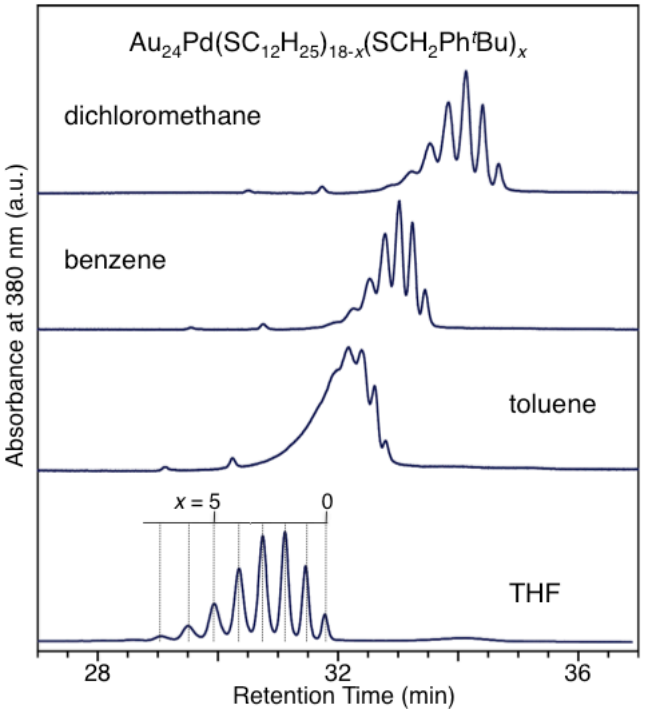

Figure S20. Elution solvent dependence of chromatograms. In these experiments, $Au_{24}Pd(SC_{12}H_{25})_{18-x}(SCH_2Ph^tBu)_x$ (x = 0–7) clusters with the distribution shown by the black line in Figure S4 were used. Methanol was used as the adsorption solvent (Chart 1). The resolutions are summarized in Table S4. The retention time order was dichloromethane > benzene > toluene > THF. In contrast, the resolution order was THF > dichloromethane > benzene > toluene (Table S4). Thus, with the gradient program in Chart 2 and methanol as the adsorption solvent, the best resolution was obtained when THF was used as the elution solvent.

References and notes

1. Deacon, M. L.; Zelakiewicz, B. S.; Tong, Y. Y. *Synlett* **2005**, 1618–1620.
2. Li, Y.; Zaluzhna, O.; Xu, B.; Gao, Y.; Modest, J. M.; Tong, Y. Y. J. *J. Am. Chem. Soc.* **2011**, *133*, 2092–2095.
3. Eti're, L. S. *Pure Appl. Chem.* **1993**, *65*, 819–872.
4. Niihori, Y.; Matsuzaki, M.; Pradeep, T.; Negishi, Y. *J. Am. Chem. Soc.* **2013**, *135*, 4946–4949.
5. Generally, the resolution of the chromatography increases with the temperature. This phenomenon has been explained by the following literature; Deemter, J. J. van, *et al*. *Chem. Eng. Sc.* **1956**, *5*, 271–289; Reid, R. C., *et al*. *The Properties of Gases and Liquids, 3d ed.*; McGraw-Hill: New York, U.S.A., 1977.
6. Negishi, Y.; Kurashige, W.; Niihori, Y.; Iwasa, T.; Nobusada, K. *Phys. Chem. Chem. Phys.* **2010**, *12*, 6219–6225.